AGU PUBLICATIONS

JGR

Journal of Geophysical Research: Solid Earth

RESEARCH ARTICLE
10.1002/2017JB014618

Key Points:
- Ultramafic pseudotachylytes may form at shallow depths during exhumation
- The magnetic properties of ultramafic pseudotachylytes inform about the oxygen fugacity at the time of seismic slip
- The magnetic properties of ultramafic pseudotachylytes reflect depth of formation

Supporting Information:
- Supporting Information S1
- Movie S1

Correspondence to:
E. C. Ferré,
eferre@geo.siu.edu

Citation:
Ferré, E. C., Meado, A. L., Geissman, J. W., Di Toro, G., Spagnuolo, E., Ueda, T., … Conder, J. A. (2017). Earthquakes in the mantle? Insights from rock magnetism of pseudotachylytes. *Journal of Geophysical Research: Solid Earth*, *122*, 8769–8785. https://doi.org/10.1002/2017JB014618

Received 7 JUL 2017
Accepted 29 OCT 2017
Accepted article online 2 NOV 2017
Published online 27 NOV 2017

Earthquakes in the Mantle? Insights From Rock Magnetism of Pseudotachylytes

Eric C. Ferré[1], Andrea L. Meado[1], John W. Geissman[2], Giulio Di Toro[3], Elena Spagnuolo[4], Tadamasa Ueda[5], Lewis D. Ashwal[6], Natalie Deseta[7], Torgeir B. Andersen[8], Justin Filiberto[1], and James A. Conder[1]

[1]Department of Geology, Southern Illinois University, Carbondale, IL, USA, [2]Department of Geosciences, University of Texas at Dallas, Richardson, TX, USA, [3]School of Earth and Environmental Sciences, University of Manchester, Manchester, UK, [4]Sezione di Sismologia e Tettonofisica, Istituto Nazionale di Geofisica e Vulcanologia, Rome, Italy, [5]Department of Earth and Planetary Science, Graduate School of Science, The University of Tokyo, Tokyo, Japan, [6]School of Geosciences, University of the Witwatersrand, Johannesburg, South Africa, [7]Planetary and Space Science Centre, University of New Brunswick, Fredericton, New Brunswick, Canada, [8]Centre of Earth Evolution and Dynamics, University of Oslo, Oslo, Norway

Abstract Ultramafic pseudotachylytes have been regarded as earthquake fossils formed at mantle depths (i.e., >30 km). Here we show that pseudotachylytes hosted by ultramafic rocks from three localities have distinct magnetic properties. Fresh host peridotites contain only small amounts of coarse-grained magnetite. In contrast, the ultramafic pseudotachylytes contain variable amounts of significantly finer magnetite that formed coseismically through melting. Among each locality, magnetite abundance in the pseudotachylytes ranges over several orders of magnitude (4–2,000 ppm), and magnetic grain size varies considerably (from single domain to multidomain). Because the host peridotites are compositionally similar, the pseudotachylyte magnetic properties are interpreted to primarily reflect the physical and cooling conditions prevailing during seismic slip. Further, the examination of laboratory-produced ultramafic pseudotachylytes shows that quenching does not produce superfine magnetite. We hypothesize that the magnetic properties of ultramafic pseudotachylytes are controlled by fO_2 and in consequence vary systematically with depth of formation. Therefore, these properties can be used to assess if the ruptures producing the earthquakes that these pseudotachylytes represent nucleated at actual mantle depths or at shallow depths during exhumation of mantle rocks.

Plain Language Summary Earthquakes generally nucleate in the upper part of the crust. A few earthquakes, however, originate in the mantle. Here we question the actual depth of seismic slip in mantle rocks. Our preliminary findings suggest that some of these rocks formed at shallower depth than previously thought.

1. Introduction

The mechanism of earthquake formation at true mantle depths in continental lithosphere is a widely studied topic in seismology (e.g., Kanamori et al., 1998). Pseudotachylytes may form by frictional melting along slip surfaces during earthquakes (Di Toro et al., 2005; Lin, 2008; Sibson, 1975). Hence, the properties of natural pseudotachylyte hosted by mantle rocks may be one of the few means of investigating seismic processes at great depths, yet how do we know at what depth such pseudotachylytes actually formed?

There are only a few ultramafic (i.e., chemical composition of peridotite) pseudotachylytes hosted by peridotites that have been reported in the literature, and previous studies have often interpreted these pseudotachylytes as evidence for seismic ruptures within the mantle while at mantle conditions (Austrheim & Andersen, 2004; Obata & Karato, 1995; Piccardo et al., 2010). Although in some cases petrologic arguments support pseudotachylyte formation at great depth (Andersen & Austrheim, 2006; Deseta, Andersen, & Ashwal, 2014a; Deseta, Ashwal, & Andersen, 2014b; Ueda et al., 2008), the presence of pseudotachylyte in ultramafic rocks does not, by itself, prove that rupturing and attending pseudotachylyte formation took place at mantle depths. Many typical melt-origin textures of pseudotachylyte result from quenching of melt and indicate disequilibrium conditions. This makes it difficult to petrologically estimate the ambient pressure and temperature conditions directly from natural pseudotachylyte. For example, the classic locality of Balmuccia, Italy, exposes a set of ultramafic pseudotachylyte veins that have

been hypothesized to have formed, based on several lines of evidence, when host mantle rocks were at 5–10 km depths or less and thus at a relatively young age in the exhumation history of these rocks (Souquière & Fabbri, 2010). Our goal is to provide independent constraints on the depth of formation of ultramafic pseudotachylytes.

We propose that the magnetic properties of ultramafic pseudotachylytes can provide a complementary means for investigating the ambient conditions of ultramafic pseudotachylyte formation. In this contribution, we use the term mantle peridotite to differentiate these rocks from crustal peridotites (i.e., ultramafic/mafic cumulate complexes). During rupture, coseismic frictional heating of mantle peridotites may lead to a rapid rise from ambient temperature (T_A) to peridotite melting temperature, i.e., solidus (T_M), accompanied by quasi-congruent melting of all silicates, although chrome spinel typically remains above the solidus (Andersen & Austrheim, 2006; Del Gaudio et al., 2009; Obata & Karato, 1995; Piccardo et al., 2010). Fusion of Fe-Mg silicates in peridotite liberates iron in the melt, and upon cooling this iron will form different Fe oxides or sulfides depending on ambient oxygen fugacity. Oxygen fugacity in the mantle is generally assumed to decrease with increasing depth (e.g., Frost & McCammon, 2008; Woodland & Koch, 2003), although significant variations are known to occur in the mantle of ocean lithosphere in subduction zones (Kelley & Cottrell, 2009). Hence, the occurrence of Fe oxides or sulfides in ultramafic pseudotachylytes likely reflects the depths of their formation. Because the compositions of any peridotitic protoliths are relatively uniform in terms of Fe content, the melting temperatures of ultramafic pseudotachylytes are similar ($T_M \approx 1{,}800$°C), and the available amount of ferrous iron will be reflected in the concentration of Fe oxides, we anticipate that variations in abundance of magnetic iron oxide phases, specifically magnetite, will be primarily caused by ambient fO_2. We also predict that magnetite abundance will be greater in ultramafic pseudotachylytes formed under higher fO_2 and thus potentially, all other parameters being equal, at shallower depths. To evaluate the setting in which ultramafic rock hosted pseudotachylytes formed, we have studied 127 samples collected from the well-studied localities of Balmuccia, and Monte Moncuni, Italy, and Cima di Gratera, Corsica. We complement this study with magnetic property data from three artificial pseudotachylytes produced under surface atmosphere conditions (variable humidity, 21% O_2) by shearing, using the rotary friction apparatus SHIVA in Rome-Istituto Nazionale di Geofisica e Vulcanologia (INGV), the Balmuccia peridotite at seismic slip rates (~1–3 m/s).

2. Geologic Setting of the Host Peridotites

All three massifs present exceptional sampling opportunities primarily because the degree of serpentinization is overall relatively low and fresh, unserpentinized domains in the ultramafic rocks are well-preserved. Also, postseismic deformation related to the exhumation of these three massifs did not impart discernible penetrative deformation to the areas where the pseudotachylyte veins are exposed.

Balmuccia - This spinel lherzolite massif, located in the Ivrea Zone of the NW Italian Alps, represents a tilted tectonic lens of pristine subcontinental lithospheric mantle, elongated subparallel to the Insubric Line (e.g., Quick et al., 1995, 2003; Rutter et al., 2007; Shervais & Mukasa, 1991). This massif equilibrated under pressures of 1.2–2.0 GPa and ambient temperature $T_A \approx 1{,}500$ K (Shervais, 1979). Olivine, orthopyroxene, clinopyroxene, and chrome spinel are the principal mineral phases, and hornblende is present in minor amounts. This region underwent a complex polyphase deformation history marked by Late Carboniferous-Early Permian transtensional uplift, Early Cretaceous transpression, and late Eocene collision (Souquière et al., 2011; Souquière & Fabbri, 2010). Pseudotachylytes commonly occur in the Ivrea Zone and cut many rock types, including metapelite, metagabbro, and peridotite host rocks (Jin et al., 1998; Matysiak & Trepmann, 2012; Obata & Karato, 1995; Pittarello et al., 2012; Souquière et al., 2011; Souquière & Fabbri, 2010; Techmer et al., 1992; Ueda et al., 2008).

Monte Moncuni - This small body forms a satellite of the Lanzo peridotite massif, located in the Piedmont of the Western Italian Alps (e.g., Piccardo et al., 2007, 2010). This relatively fresh massif originated from an extended subcontinental lithospheric mantle that was subsequently modified by mid-ocean ridge basalt-type melts during the Jurassic opening of the Tethyan Ocean. The lherzolites at Monte Moncuni are plagioclase-impregnated and show important deformational features marked by shear zones, cataclastic bands, and the production of pseudotachylytes, both as generation and injection veins (Piccardo et al., 2010).

Cima di Gratera - This massif consists of variably serpentinized plagioclase and spinel lherzolite in contact with a leucocratic and variably preserved metagabbro that both form part of the Schistes Lustrés units of northern Corsica (e.g., Austrheim & Andersen, 2004). The Schistes Lustrés units are interpreted as dismembered ocean lithosphere ophiolitic slices that underwent blueschist to lawsonite eclogite facies metamorphism during Late Cretaceous to early Cenozoic subduction, under peak conditions of 1.5 to 2.6 GPa and $T_A \approx 850$ K (Lahondère, 1988; Ravna et al., 2010; Vitale-Brovarone et al., 2013).

Artificial ultramafic pseudotachylytes - The artificial pseudotachylytes were produced by shearing solid cylinders (50 mm in diameter) of a sample of Balmuccia spinel lherzolite (see Del Gaudio et al., 2009, for rock description). This peridotite is massive, free from macroscopic fractures and veins, and was collected from a quarry located ≈200 m northeast from the Balmuccia pseudotachylyte outcrop described in Obata and Karato (1995). The specimens were slid under normal atmospheric conditions, i.e., room humidity conditions and ≈21% O_2, at 2.5 m/s for about 20 m under a normal stress of 6.3 MPa, using the rotary shear apparatus SHIVA at Roma-INGV (supporting information Video S1; Di Toro et al., 2010; Niemeijer et al., 2011; Nielsen, 2011). Solidified melt drops were centrifugally ejected from the slipping zone during frictional sliding and melting; they were recovered from experiments 1205, 1208, and 1209 for microstructural and magnetic analysis (Table 1).

3. Macroscopic, Petrographic, and Microstructural Characteristics of Pseudotachylytes

In this paper we refer to the main fault surfaces along which melt is primarily formed and preserved as generation veins and to those branching off the main veins as injection veins (e.g., Ferré et al., 2005a).

The following is a summary of previous work, complemented by our own field, macroscopic and microscopic observations based on a collection of 104 fresh specimens of pseudotachylytes hosted by ultramafic rocks. In the field, we used an electric 12.7 mm diameter drill to selectively sample unaltered material. Most of our samples originated from generation veins between 10 and 20 mm in thickness. Samples previously investigated and provided by Ashwal, Austrheim, and Ueda are named as such in Table 1. Our samples were examined with a petrographic microscope (24 thin sections) as well as a scanning electron microscope coupled with an energy dispersive system for elemental analyses (supporting information).

The color of fresh vein material is typically very dark gray with bluish hues, whereas altered material tends to have dark green hues. In addition, the magnetic susceptibility of ultramafic material is a good proxy for serpentinization, because serpentinization generally produces abundant magnetite (e.g., Toft et al., 1990), and was used to select fresh material. We show that the mineral assemblages and microstructures of pseudotachylyte veins vary significantly among the three studied localities. In all localities, the clast/matrix ratio, however, remains remarkably constant at about 5–10%, with the exception of one sample (≈20%) (Cima di Gratera, sample COR006).

Balmuccia - The Balmuccia pseudotachylytes consist of at least two successive sets of veins, initially investigated by Obata and Karato (1995), Ueda et al. (2008), and Souquière and Fabbri (2010). We follow the structural classification of Souquière and Fabbri (2010) and complement it with our own observations: *A-type* veins (e.g., BAL019; Figure 1a) consist of ≈1 to 20 mm thick steeply oriented generation veins, more than 10 m in length (based on available exposure), as well as rare injection veins, up to 5 mm in length. These veins sharply crosscut banding, websterite dikes, and folds in banding, producing offsets of up to 3 m. Some veins display mylonitic reactivated margins as shown by crystal-plastic deformation in host silicates (Ueda et al., 2008). These veins show a foliation marked by the alignment of microcrystallites in the matrix. The veins also contain fine-grained (5–10 μm) olivine and clinopyroxene (<5% of the total clast volume) clasts, with rounded shapes and similar sizes, as well as very fine (<5 μm) chrome spinel clasts. At the thin-section scale, the clast-to-matrix ratio varies considerably along and across each vein. Clinopyroxene in the matrix forms dendritic and skeletal crystals. Orthopyroxene (enstatite) is a rare phase as a matrix mineral but is more common as clasts. The vein contacts with their peridotite host rocks are typically sharp along one margin, but in several cases the opposite host rock margin shows mylonitic deformation. This type of vein grades into ultramylonite along strike, where clasts tend to be larger (>20 μm). These pseudotachylytes formed under a pressure ≈1.0–1.3 GPa and $T_A \approx 1{,}100$ K (Ueda et al., 2008). *B-type* veins (e.g., BAL015; Figures 1b and 1d) consist of ≈10 to 25 mm thick generation veins, up to 7 m in length, and relatively extensive injection veins up to

Table 1
Magnetic Hysteresis Properties of Ultramafic Pseudotachylytes

	Sample no.	Mass (g)	M_s (mAm^2)	M_r (mAm^2)	H_c (mT)	H_{cr} (mT)	M_r/M_s	H_{cr}/H_c	ppm Mag	Khf (10–6 [SI])
Balmuccia A-type	BAL019A	0.240	0.932	0.268	35.8	58.7	0.288	1.641	4.2	857
	BAL019D	0.240	0.091	0.027	20.4	73.7	0.293	3.605	4.1	681
	BAL019E	0.250	0.072	0.029	13.6	149.4	0.399	11.010	3.1	593
	BAL019F	0.270	0.092	0.031	16.7	75.3	0.334	4.510	3.7	609
	BAL019H	0.250	0.068	0.019	14.5	64.0	0.282	4.399	2.9	601
	BAL019I	0.200	0.068	0.044	20.4	202.1	0.647	9.926	3.7	608
	BAL019J	0.170	0.098	0.060	32.8	144.3	0.610	4.399	6.3	671
	UedaBM9322A	0.360	0.126	0.094	58.9	121.0	0.752	2.055	3.8	578
	UedaBM9322C	0.430	0.215	0.130	62.3	100.5	0.606	1.613	5.4	562
	UedaBM9322E	0.450	0.156	0.116	77.1	115.2	0.743	1.493	3.8	450
	UedaBM9322F	0.380	0.219	0.114	71.7	131.3	0.519	1.832	6.3	617
	UedaBM9322G	0.370	0.157	0.110	63.3	151.0	0.696	2.387	4.6	557
	Min	0.170	0.068	0.019	13.6	58.7	0.282	4.322	2.9	450
	Max	0.450	0.932	0.268	77.1	202.1	0.288	2.620	6.3	857
	Average	0.301	0.191	0.087	40.6	115.5	0.454	2.844	4.3	615
	Median	0.260	0.112	0.077	34.3	118.1	0.689	3.446	3.9	605
Balmuccia B-type	BAL016A	0.340	157.300	21.150	10.8	22.2	0.134	2.066	5028.8	509
	BAL016B	0.330	194.204	30.531	10.2	17.8	0.157	1.756	6396.7	478
	BAL016C	0.380	157.995	20.774	10.7	23.2	0.131	2.178	4519.3	491
	BAL018A	0.450	63.506	14.376	26.0	50.3	0.226	1.939	1534.0	321
	BAL018B	0.330	50.873	12.617	30.9	61.6	0.248	1.995	1675.6	1016
	BAL018C	0.190	31.039	8.593	35.8	63.8	0.277	1.782	1775.7	653
	BAL018D	0.260	15.416	3.726	34.4	70.8	0.242	2.060	644.5	419
	BAL018E	0.220	49.745	11.069	27.4	56.3	0.223	2.052	2457.7	750
	BAL018F	0.260	69.936	16.670	28.3	54.4	0.238	1.922	2923.7	667
	BAL018G	0.240	26.301	6.798	30.2	57.2	0.258	1.894	1191.2	706
	BAL018H	0.180	15.815	4.213	35.4	67.3	0.266	1.904	955.0	591
	BAL018I	0.240	48.297	12.859	33.5	61.2	0.266	1.824	2187.4	614
	BAL018J	0.290	21.639	5.969	38.6	71.1	0.276	1.840	811.0	488
	BAL018L	0.320	77.306	16.531	25.5	51.2	0.214	2.007	2626.4	606
	BAL018M	0.240	2.931	0.912	44.2	82.9	0.311	1.875	132.7	123
	BAL018N	0.320	36.453	10.203	36.6	67.0	0.280	1.828	1238.2	450
	BAL018O	0.141	18.704	4.922	37.4	71.4	0.263	1.910	1441.9	587
	BAL018P	0.240	18.614	5.614	40.4	71.7	0.302	1.773	843.0	552
	BAL018Q	0.180	15.393	4.089	37.8	71.1	0.266	1.882	929.6	554
	BAL018R	0.300	34.197	8.278	29.0	56.5	0.242	1.948	1239.0	456
	BAL018S	0.210	19.270	5.916	40.1	68.2	0.307	1.701	997.4	574
	Min	0.141	2.931	0.912	10.2	17.8	0.311	1.756	132.7	123
	Max	0.450	194.204	30.531	44.2	82.9	0.157	1.875	6396.7	1016
	Average	0.270	53.568	10.753	30.6	58.0	0.201	1.893	1978.5	553
	Median	0.260	34.197	8.593	33.5	61.6	0.251	1.837	1441.9	554
Monte Moncuni	MON001A	0.270	0.594	0.219	37.2	102.9	0.370	2.770	23.9	502
	MON001B	0.250	0.674	0.287	37.0	83.2	0.425	2.248	29.3	598
	MON001C	0.240	0.662	0.282	39.2	88.3	0.426	2.251	30.0	592
	MON001D	0.250	1.138	0.473	29.9	65.7	0.416	2.199	49.5	541
	MON001E	0.250	0.595	0.253	45.5	92.0	0.425	2.023	25.9	565
	MON001F	0.260	1.070	0.456	30.2	75.9	0.427	2.511	44.7	559
	MON001H	0.200	0.895	0.306	29.4	65.1	0.342	2.219	48.7	608
	MON003A	0.160	0.932	0.449	39.6	79.4	0.481	2.005	63.3	678
	MON003B	0.240	1.071	0.534	37.6	70.8	0.498	1.882	48.5	574
	MON003C	0.220	1.792	0.666	33.6	69.6	0.372	2.072	88.5	666
	MON003D	0.230	2.104	0.806	32.7	66.8	0.383	2.046	99.4	601
	MON003E	0.210	1.476	0.598	38.6	70.5	0.405	1.828	76.4	607
	MON003F	0.250	1.841	0.672	41.2	66.6	0.365	1.616	80.0	600
	MON003G	0.220	1.359	0.624	36.8	64.3	0.459	1.746	67.1	680
	MON003H	0.200	0.651	0.314	35.4	71.3	0.483	2.012	35.4	599
	MON003I	0.240	0.981	0.487	38.5	73.1	0.496	1.899	44.4	632
	MON005A	0.350	0.490	0.199	26.6	60.4	0.405	2.275	15.2	439
	MON005B	0.340	0.369	0.110	28.6	60.1	0.297	2.100	11.8	438
	MON005C	0.360	1.018	0.410	26.0	51.0	0.403	1.962	30.7	544

Table 1. (continued)

	Sample no.	Mass (g)	M_s (mAm^2)	M_r (mAm^2)	H_c (mT)	H_{cr} (mT)	M_r/M_s	H_{cr}/H_c	ppm Mag	Khf (10–6 [SI])
	MON005D	0.410	0.494	0.237	29.9	70.3	0.480	2.348	13.1	529
	MON005E	0.330	0.408	0.247	33.1	90.3	0.605	2.730	13.4	621
	MON005F	0.360	0.605	0.284	26.6	60.7	0.470	2.282	18.3	570
	MON005G	0.350	0.358	0.183	29.8	73.2	0.512	2.453	11.1	538
	Min	0.160	0.358	0.110	26.0	51.0	0.306	1.962	11.1	438
	Max	0.410	2.104	0.806	45.5	102.9	0.383	2.264	99.4	680
	Average	0.269	0.938	0.395	34.0	72.7	0.422	2.135	42.1	577
	Median	0.250	0.895	0.314	33.6	70.5	0.351	2.096	35.4	592
Cima di Gratera	COR006A	0.520	2.820	1.127	34.0	68.9	0.400	2.027	58.9	501
	COR006B	0.590	2.679	0.935	30.7	71.1	0.349	2.313	49.4	481
	COR006C	0.660	3.066	1.559	41.3	69.7	0.508	1.688	50.5	551
	COR006D	0.690	2.435	1.497	45.8	72.8	0.615	1.588	38.4	601
	COR006E	0.640	2.087	1.309	46.1	76.1	0.627	1.651	35.4	594
	COR006F	0.710	4.029	2.117	41.7	66.3	0.525	1.589	61.7	640
	COR006G	0.750	2.232	1.016	31.2	69.6	0.455	2.231	32.3	404
	COR006H	0.780	2.123	0.891	30.5	65.4	0.420	2.145	29.6	397
	COR006I	0.930	2.459	1.157	29.3	69.5	0.471	2.372	28.7	416
	COR006J	0.930	2.873	1.107	24.3	54.9	0.385	2.253	33.6	401
	COR006K	0.650	5.240	1.790	18.1	43.6	0.342	2.406	87.6	548
	COR006L	0.650	2.546	1.007	31.4	66.8	0.396	2.130	42.6	512
	COR006M	0.670	2.183	1.024	40.3	70.8	0.469	1.758	35.4	533
	COR006N	0.820	2.435	1.337	39.5	67.4	0.549	1.706	32.3	582
	COR006O	0.920	2.374	0.844	22.3	51.0	0.355	2.289	28.1	319
	COR006P	0.780	2.649	1.344	35.0	60.7	0.507	1.735	36.9	514
	COR006Q	0.740	2.758	1.016	26.2	60.0	0.369	2.288	40.5	515
	COR006R	0.640	2.905	1.048	24.3	53.9	0.361	2.215	49.3	538
	COR006S	0.770	2.130	0.737	18.5	41.5	0.346	2.243	30.1	276
	COR006T	0.620	1.494	0.645	27.6	57.9	0.432	2.099	26.2	382
	AndersenCOR25-05A	0.210	6.939	2.653	27.5	46.1	0.382	1.674	359.2	643
	AndersenCOR25-05B	0.230	4.559	2.047	32.7	51.7	0.449	1.582	215.5	613
	AndersenCOR25-05C	0.210	8.157	3.100	27.4	45.8	0.380	1.672	422.2	650
	AndersenCOR25-05D	0.260	7.890	3.363	32.9	53.7	0.426	1.635	329.9	636
	AndersenCOR25-05E	0.240	5.324	2.175	28.9	49.1	0.409	1.698	241.1	622
	AndersenCOR25-05F	0.240	3.192	1.496	33.1	51.1	0.469	1.544	144.6	367
	AndersenCOR25-05G	0.200	2.647	1.181	29.1	48.1	0.446	1.651	143.9	595
	AndersenCOR25-05H	0.220	3.884	1.646	27.8	44.4	0.424	1.598	191.9	594
	AndersenCOR25-05I	0.200	2.188	0.921	28.3	45.3	0.421	1.597	118.9	589
	AndersenCOR25-05 J	0.220	2.608	1.217	29.7	49.4	0.467	1.662	128.8	595
	AndersenCOR25-05 K	0.250	2.171	0.953	25.5	44.1	0.439	1.732	94.4	599
	AshwalPST12A	0.330	13.438	4.241	30.1	57.5	0.316	1.908	442.6	593
	AshwalPST12B	0.300	13.068	4.397	31.3	53.3	0.336	1.704	473.5	514
	AshwalPST12C	0.340	20.172	6.948	27.7	52.2	0.344	1.883	644.9	581
	AshwalPST12D	0.290	20.755	5.567	27.0	56.4	0.268	2.092	777.9	749
	AshwalPST12E	0.360	14.177	5.149	32.9	54.2	0.363	1.650	428.1	651
	AshwalPST12F	0.250	10.167	3.559	20.2	48.1	0.350	2.377	442.0	823
	AshwalPST12G	0.270	10.233	3.732	27.8	55.2	0.365	1.986	412.0	875
	AshwalPST12H	0.310	36.491	9.774	20.4	46.7	0.268	2.288	1279.5	617
	AshwalPST12I	0.210	6.736	2.179	30.1	53.7	0.323	1.781	348.7	653
	AshwalPST12J	0.300	14.805	5.123	31.1	52.5	0.346	1.687	536.4	579
	AshwalPST12K	0.250	7.755	2.828	33.1	55.6	0.365	1.677	337.2	535
	AshwalPST12L	0.260	15.125	5.204	31.6	53.0	0.344	1.677	632.3	587
	Min	0.200	1.494	0.645	18.1	41.5	0.432	2.289	26.2	276
	Max	0.930	36.491	9.774	46.1	76.1	0.268	1.651	1279.5	875
	Average	0.475	6.651	2.394	30.3	56.4	0.360	1.859	231.9	557
	Median	0.340	3.066	1.497	30.1	53.9	0.488	1.790	118.9	582
Exp.	S1205	0.186	1.229	0.237	23.4	50.4	0.193	2.154	68.6	285
	S1208	0.175	1.548	0.756	21.5	30.2	0.488	1.400	93.4	471
	S1209	0.110	1.605	0.442	24.3	54.8	0.275	2.258	158.6	673

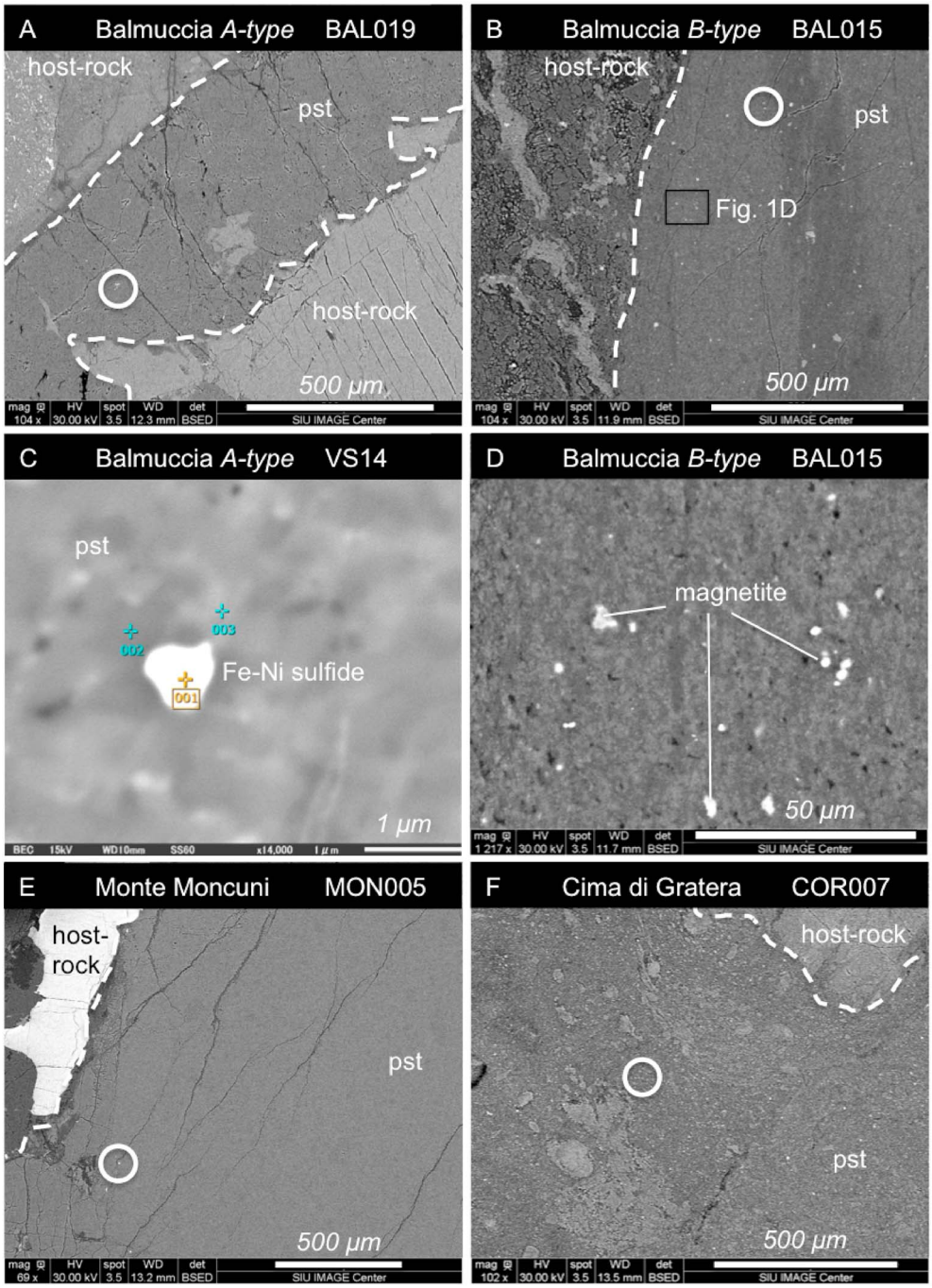

Figure 1. Back-scattered electron microscopic image of ultramafic pseudotachylytes documenting the small size, dissemination, and morphology of primary magnetite and sulfide grains. (a) Balmuccia A-type, Italy; (b) Balmuccia B-type, Italy; (c) Balmuccia A-type showing a small Fe-Ni sulfide grain; (d) Balmuccia B-type, close-up of Figure 1b showing magnetite grain subrounded to subhedral morphology; (e) Monte Moncuni, Italy; and (f) Cima di Gratera, Corsica. The white circles represent locations of magnetite grain (bright).

1.5 m in length. These B-type generation veins are subhorizontal and located within hydrous-mineral-bearing shear zones (Handy & Stünitz, 2002). These later veins generally have a glassy aspect and distinct spherulitic microstructures. The perfect optical isotropy and homogeneity of the material indicate that this brown glass is not devitrified. Spherical vesicles filled with dolomite and talc, up to 150 μm in diameter, occur in the glassy zones. The fluid responsible for vesiculation might have originated from amphibole breakdown. These veins formed at even lower pressures ≈0.15–0.30 GPa and T_A ≈ 450–600 K (Souquière & Fabbri, 2010).

Monte Moncuni - The Monte Moncuni pseudotachylytes (e.g., MON005; Figure 1e) consist of centimeter-wide generation veins and injection veins up to 0.5 m in length (e.g., Piccardo et al., 2010). The generation veins broadly parallel the plagioclase lherzolite mylonitic foliation over tens of meters. All veins exhibit sharp contacts with the host rocks, and many generation veins have a high aspect ratio, with lensoidal shape. A few generation veins host macroscopically visible vesicles ($<$0.5 mm). The pseudotachylytes consist of ultrafine-grained matrix and up to 15% olivine clasts. Microstructures such as radial aggregates of orthopyroxene microcrystallites ($<$0.5 mm in diameter) and spherulitic microstructures attest to the melt origin of these pseudotachylytes. Geologic and petrologic observations constrain the depth of formation to $\leq$0.5 GPa and $T_A \approx 900$ K (Piccardo et al., 2010).

Cima di Gratera - The Cima di Gratera pseudotachylytes (e.g., COR007; Figure 1f) occur in both metagabbros and peridotites (e.g., Andersen et al., 2008; Andersen et al., 2014; Andersen & Austrheim, 2006; Austrheim & Andersen, 2004; Deseta et al., 2014a; Deseta et al., 2014b; Magott et al., 2016, 2017), although the following observations pertain to ultramafic veins only. The ultramafic pseudotachylytes form extensive (tens of meters long), relatively thick generation veins (generally $<$15 mm, but up to 300 mm) and also a thick (up to 6 m), nonhierarchical net-vein complex with up to 50% ultramafic pseudotachylyte. The thickest generation veins and the net-vein complex are generally parallel to the subhorizontal gabbro-peridotite contact (Andersen et al., 2014; Magott et al., 2017). A second set of steeply dipping (≈55°) pseudotachylyte generation veins, which are up to 0.3 m in thickness, occurs in the peridotites away from the gabbro-peridotite contact. These veins can be traced tens of meters through well-preserved peridotites until they are fragmented by deformation associated with the serpentinization that occurs around peridotite bodies. The main serpentinization event(s) postdates frictional melting, as shown by serpentinized microcrystallites (e.g., Magott et al., 2016), although some serpentinization predates seismic slip. Magnetite forms mostly subhedral grains of 3 to 5 μm in diameter (in white circles in Figure 1) that are evenly disseminated throughout the vein. In some thin sections, magnetite also forms rim-overgrowth on nonmelted chrome spinel clasts (Andersen & Austrheim, 2006, Figures 5b and 5d). Some veins exhibit mineral filled vesicles (up to 2 mm in diameter) that, in some cases, are elongated subparallel to the vein margins. Some fault generation veins preserve thin ($<$1 mm) wall-rock damage zones, locally truncated by small pseudotachylyte injection veins. Microtextural studies, including electron backscatter diffraction, suggest that in these damage zones the wall-rock olivine was deformed by crystal plasticity. This in turn localized deformation and contributed to weakening and pseudotachylyte faulting. This indicates that the weakening mechanism for these earthquakes within ultramafic rocks was a thermal run-away process (Deseta et al., 2014b; John & Schenk, 2006; Silkoset, 2013). The ambient conditions of seismic slip are estimated to have been 1.8–2.6 GPa and $T_A \approx$ 700–800 K (Deseta et al., 2014a; Ravna et al., 2010).

Friction experiment materials - Centrifugally ejected frictional melt (glass) was retrieved from three distinct runs 1205, 1208, and 1209, all at 6.3 MPa normal stress conditions, similar to the experiments of Del Gaudio et al. (2009). All experiments were performed, within 10 to 13 s, under uncontrolled atmosphere (O_2 concentration ≈ 21%).

4. Magnetic Properties of Ultramafic Pseudotachylytes

Thermomagnetic analyses, magnetic hysteresis measurements, isothermal remanent magnetization (IRM) acquisition experiments, and first-order reversal curve (FORC) analyses were systematically performed on small cubical specimens (0.14–0.93 g) of clast-poor, ultramafic pseudotachylyte from the three localities above, as well as the artificially produced pseudotachylytes. The results are presented below according to the following groups of specimens: Balmuccia A-type, Balmuccia B-type, Monte Moncuni, Cima di Gratera, and artificial pseudotachylytes. Methods are described in detail in the supporting information.

The specimens used for this study are unaltered and consist primarily of a fine-grained matrix of olivine, clinopyroxene, orthopyroxene, plagioclase, and magnetite, with a few clasts of chrome spinel. We consider likely origins of the magnetite grains in section 5. At room temperature, ferromagnesian silicates and chrome spinel are paramagnetic, while plagioclase is diamagnetic (e.g., Lagroix & Borradaile, 2000; Dunlop & Özdemir, 2009; Ferré, Zechmeister, et al., 2005; Ferré, Friedman, et al., 2014; Ferré, Geissman, et al., 2014). Magnetite, the only ferromagnetic (*s.l.*) phase in these pseudotachylytes, was identified through optical and backscatter electron microscopy. The low Ti content of magnetite is determined

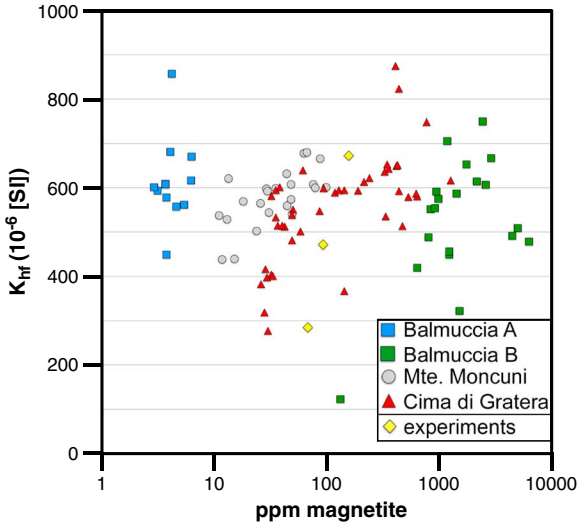

Figure 2. Plot of high-field magnetic susceptibility (K_{hf}), determined from magnetic hysteresis experiments, versus magnetite concentration (in ppm), determined from the magnetic saturation of ultramafic pseudotachylyte specimens. The four groups of natural specimens and artificial specimens display distinct magnetic properties that reflect different fO_2 conditions during frictional melting at different depths. Low fO_2 results in low magnetite contents, whereas high fO_2 results in high magnetite content.

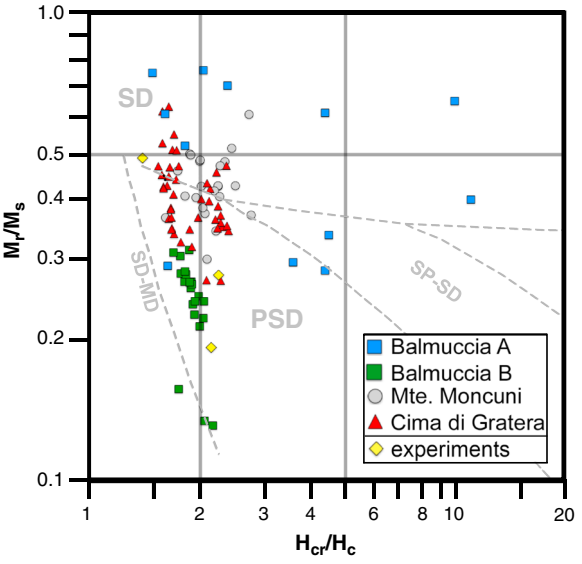

Figure 3. Plot of M_r/M_s versus H_{cr}/H_c (plot of Day et al., 1977, as modified by Dunlop, 2002) for natural and artificial pseudotachylytes studied in this paper. Both hysteresis parameters M_r/M_s and H_{cr}/H_c are concentration-independent and directly reflect different magnetite grain size populations. All groups define broad mixing trends between single domain (SD) and pseudo-single domain (PSD) grain sizes. The scatter of points from Balmuccia A is most likely due to low magnetite content. The dashed lines are from Dunlop (2002).

from both (1) thermomagnetic analyses, through Curie temperatures (T_c) between 566 and 577°C, which yielded mole percentages of ulvöspinel component (x_{ulv}) ranging between 2.1 and 0.2 ± 0.1% (supporting information), and (2) energy dispersive spectroscopy (EDS) spot analyses, which yielded x_{ulv} between 0.28 and 0.17 ± 0.02%. The thermomagnetic experiments (supporting information) also display a significant reversibility of heating and cooling curves, which is consistent with pure magnetite being the dominant ferromagnetic phase. Thermomagnetic experiments, IRM acquisition experiments, and the fact that specimens reach magnetic saturation at relatively low fields ($H_s < 200$ mT) all demonstrate that magnetite is the only ferromagnetic (*s.l.*) phase present in these rocks and experimental materials.

The magnetic hysteresis experiments provide information on both concentration-dependent parameters, such as M_s (saturation magnetization), M_r (saturation remanence), and K_{hf} (high-field magnetic susceptibility), and concentration-independent parameters, such as H_c (magnetic coercivity) and H_{cr} (coercivity of remanence) (Evans & Heller, 2003). The magnetic hysteresis properties (Table 1 and Figure 2) reflect great variability in both magnetite concentration and magnetite grain size. Overall, in the natural specimens, magnetite concentration ranges between ≈2.9 and ≈6,400 ppm and was calculated from the known saturation magnetization of magnetite, M_s = 92 Am^2/kg (Tauxe, 1998), and the measured saturation magnetization (Table 1). The Balmuccia B-type veins (green squares on Figure 2) show the highest magnetite abundance (average ≈ 1,978 ppm). The Cima di Gratera veins (red triangles on Figure 2) display the second highest magnetite abundances (average ≈ 232 ppm). The Monte Moncuni veins (grey circles on Figure 2) exhibit moderate magnetite abundances (average ≈ 42 ppm). The Balmuccia A-type veins (blue squares on Figure 2) have the lowest magnetite abundances (average 4 ppm). The specimens therefore define four distinct groups of magnetite contents. In contrast, the values of K_{hf} show relatively modest variations (Table 1 and Figure 2). K_{hf} represents the sum of diamagnetic (plagioclase) and paramagnetic (olivine, pyroxenes, and chrome spinel) contributions to magnetic susceptibility. Plagioclase occurs in low percentages (<5%) and has a very small, negative magnetic susceptibility (-14.9×10^{-6} [supporting information]; Dunlop & Özdemir, 2009). Hence, K_{hf} reflects primarily paramagnetic susceptibility (i.e., the magnetic susceptibility due to paramagnetic minerals). The maximum theoretical paramagnetic magnetic susceptibility (K_{para}) of a rock is dependent on its composition (mainly Fe, Mn, Ni, and Co contents). Using Syono's (1960) empirical formula, published peridotite geochemical analyses from the same localities, and following the approach of Aydin et al. (2007), we obtain $K_{para} = 559 \pm 22 \times 10^{-6}$ [supporting information], $565 \pm 40 \times 10^{-6}$ [supporting information], and $580 \pm 16 \times 10^{-6}$ [supporting information], respectively, for Balmuccia, Monte Moncuni, and Cima di Gratera (supporting information Table S1).

Magnetite grain size is evaluated using the M_r/M_s and H_{cr}/H_c ratios, using the plot of Day, Fuller, and Schmidt (1977), as modified by Dunlop (2002) (Figure 3). General background on the physical interpretation of hysteresis loops can be found in Tauxe et al. (2002). Overall, in this diagram, magnetic granulometry increases from top-left single domain (SD) to bottom-right multidomain (MD), and each set of specimens forms well-defined clusters. The median values of the squareness ratio (M_r/M_s) are 0.689, 0.488, 0.351, and 0.251, respectively, for Balmuccia A-type, Cima di Gratera, Monte

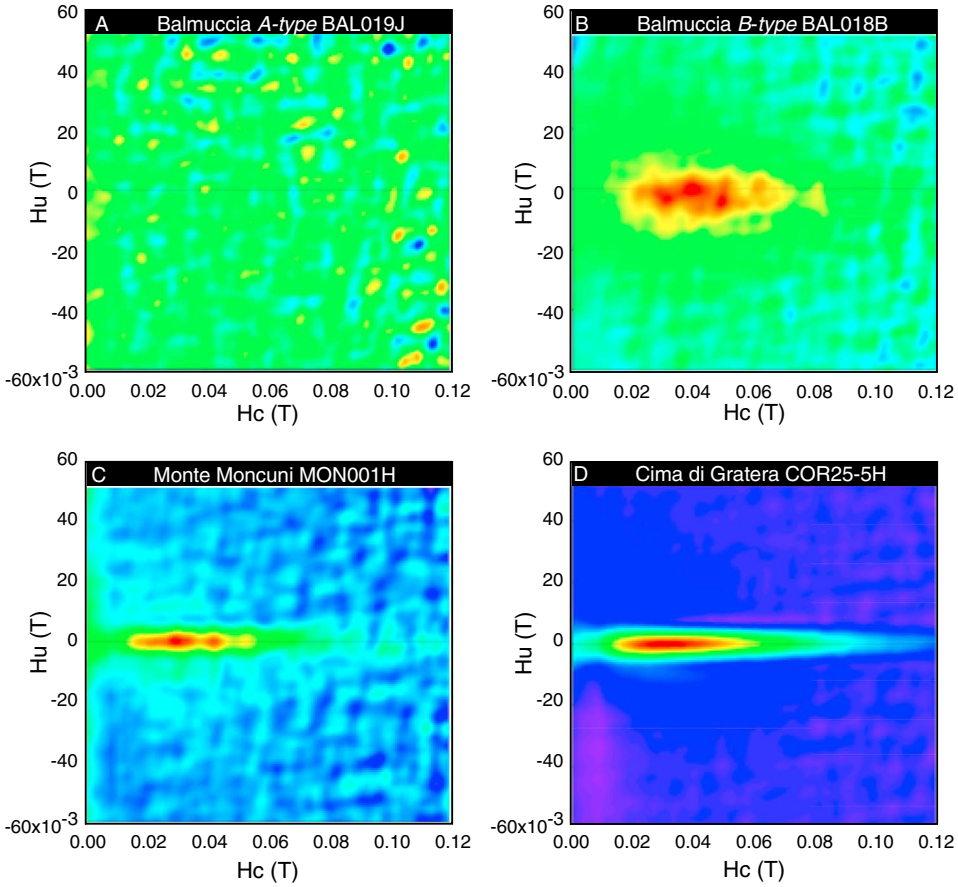

Figure 4. First-order reversal curves (FORC) of ultramafic pseudotachylyte specimens. (a) Balmuccia A-type, Italy; (b) Balmuccia B-type, Italy; (c) Monte Moncuni, Italy; and (d) Cima di Gratera, Corsica. The low concentrations in Balmuccia A-type do not result in a legible FORC diagram, whereas in other groups, noninteracting populations of grains show magnetic coercivity ranging between 20 and 40 mT. This shows the absence of high coercivity phases such as goethite, maghemite, or hematite and is consistent with magnetite as the main ferromagnetic phase.

Moncuni, and Balmuccia B-type samples. With one exception, the arrays characterized by each population fall along those defined experimentally by Dunlop (2002) as mixtures of SD and MD grains, most likely due to the range of magnetite grain sizes in these rocks. The Balmuccia A-type data, however, do not exhibit this behavior and plot along a trend generally attributed to mixtures between SD and superparamagnetic (SP) grains.

First-order reversal curve (FORC) diagrams can be used to constrain the bulk distribution of magnetic grain sizes in a specimen (e.g., Roberts et al., 2014). Representative examples of FORC analyses for the four groups of pseudotachylytes are given in Figure 4. The Balmuccia A-type pseudotachylytes, being dominated by paramagnetic minerals and hosting only trace amounts of fine magnetite, do not yield meaningful FORC results (Figure 4a). For the other three localities, Balmuccia B-type, Monte Moncuni, and Corsica, FORC diagrams point to a single-phase, uniform distribution of noninteracting grains (Figures 4b–4d). For these localities, the mean magnetic coercivity (H_c) falls in the 20 to 50 mT range, with a mean around 30 mT, in agreement with values obtained from the major hysteresis loops (Table 1). These ultramafic pseudotachylytes show FORC similarities to pseudotachylytes derived from quartzo-feldspathic/tonalitic host rocks (e.g., Ferré et al., 2012; Ferré, Friedman, et al., 2014 and Ferré, Geissman, et al., 2014). The H_c parameter varies in a range typical for stoichiometric magnetite and further confirms the absence of highly oxidized phases such as hematite. The Curie temperatures near 577°C (supporting information) indicate the absence of maghemite in our samples.

Isothermal remanent magnetization (IRM) curves acquired for representative samples are shown in Figure 5. These curves show smooth, concave downward curvatures indicating that a single magnetic phase dominates the remanence. These experiments also confirm the variations in magnetic grain sizes

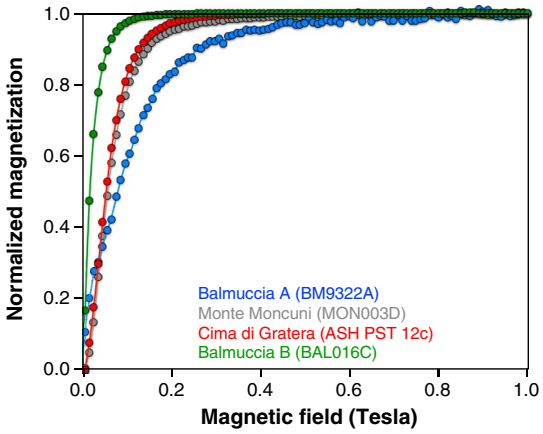

Figure 5. Isothermal remanent magnetization (IRM) curves acquired for representative samples of the four localities.

observed in the Dunlop (2002) plot of Figure 3, with Balmuccia A being finer grained than Balmuccia B. We have utilized the Max Unmix IRM deconvolution Web application (Maxbauer et al., 2016) to attempt to better evaluate the magnetic mineral components to the pseudotachylytes studied. With the exception of the Balmuccia A specimens, our most reasonable decompositions identify a single magnetic component with a relatively low coercivity (~30 mT) and a low residual sum square estimate. The three specimens produced by friction experiments yield magnetic properties similar to those of natural specimens, particularly the Balmuccia B-type and Cima di Gratera specimens. The magnetite contents in the artificial specimens have a limited variation between ≈69 and 160 ppm, whereas greater variation occurs in K_{hf} between ≈285 and 673 × 10^{-6} [SI]. The small size of the specimens probably increases instrumental uncertainties. The grain size sensitive magnetic parameters point to a similarity with natural samples and fall in the pseudo-single domain (PSD) field.

5. Discussion

During rupture and seismic motion, comminuted clasts of the host rock are embedded in a frictional melt (Maddock, 1983; Shimamoto & Nagahama, 1992; Sibson & Toy, 2006). In pseudotachylytes, the clasts primarily maintain the magnetic properties of the host rock. In contrast, the melt quenches and crystallizes a fine-grained matrix that exhibits properties that are dictated by the melting and cooling conditions (e.g., Ferré et al., 2012; Tanikawa et al., 2008).

5.1. Magnetite in the Host Peridotites Before Seismic Slip (i.e., Pseudotachylyte Formation)

In general, our understanding of fO_2 in the upper mantle derives mainly from detailed investigations of ultramafic xenoliths because these materials ascend rapidly through the lithosphere (e.g., Demouchy et al., 2006; Peslier et al., 2008), and hence constitute the best available record of petrologic conditions in the mantle (e.g., Nixon, 1987). Previous studies considered magnetite a rare primary phase in pristine, unaltered mantle peridotites (e.g., Wasilewski, 1987; Wasilewski & Mayhew, 1992; Wasilewski et al., 1979). This view has recently been challenged by new data on fresh mantle xenoliths that demonstrates the presence of primary, pure (i.e., $x_{ulv} = 0$) magnetite, albeit in low concentration, in these rocks (Ferré et al., 2013; Ferré, Friedman, et al., 2014; Ferré, Geissman, et al., 2014; Friedman et al., 2014; Martin-Hernandez et al., 2014). These results show that primary magnetite can be present in the upper mantle, in the absence of serpentinization, reflecting conditions above the wüstite-magnetite oxygen buffer, as predicted by Frost and McCammon (2008) and Goncharov et al. (2012).

In the case of the three massifs hosting ultramafic pseudotachylytes that we have studied (Balmuccia, Monte Moncuni, and Cima di Gratera peridotites), assessing fO_2 and the possible presence of magnetite in the host rock before rupture and pseudotachylyte formation is difficult. Both serpentinization and talcification that took place prior to coseismic pseudotachylyte faulting were documented in the case of the Cima di Gratera (Austrheim & Andersen, 2004, Figure 3). Indeed, all three massifs have also undergone complex postseismic, tectonic histories during which magnetite could have formed in the host peridotite. The three main processes that could form small concentrations of magnetite, at mantle depths (i.e., >30 km), in the preseismic host peridotite are (i) serpentinization, i.e., fluid-present reactions that produce serpentine and magnetite from olivine and pyroxene (direct evidence for serpentinization at mantle depths is uncommon; e.g., Facer et al., 2009; Smith, 2010); (ii) pervasive interaction with basaltic melts, a well-known process in mantle xenoliths during ascent (e.g., Kinman & Neal, 2006; Taylor & Neal, 1989), but far less likely for peridotite massifs; and (iii) oxidation of olivine, a reaction that forms magnetite by solid state iron diffusion within grains (e.g., Kohlstedt et al., 1976; Putnis, 1979). Although all three processes could have taken place at the pseudotachylyte localities, the most likely scenario to produce magnetite in nonmetasomatized upper mantle rocks is the third one, that of solid-state oxidation, because these massifs are remarkably weakly serpentinized (e.g., Austrheim & Andersen, 2004; Obata & Karato, 1995;

Piccardo et al., 2010), especially compared to other ultramafic massifs (e.g., Feinberg et al., 1999; Frost et al., 2013; Hyndman & Peacock, 2003; Malvoisin et al., 2012; Moody, 1976; O'Driscoll & Petronis, 2009). Furthermore, the dikes that cut through the host peridotites, and attest to melt migration, are pyroxenitic in composition and, unlike dikes of mafic composition, would not lead to magnetite nucleation (Shervais & Mukasa, 1991; Piccardo et al., 2010).

A postseismic origin for magnetite can be ruled out for three main reasons: (i) magnetite grains are elongated parallel to the viscous flow fabric of the pseudotachylyte and carry an AMS fabric that is kinematically consistent with coseismic slip, at least in the case of Cima di Gratera (Ferré et al., 2016); (ii) in contrast to other pseudotachylytes (Ferré, Friedman, et al., 2014 and Ferré, Geissman, et al., 2014), the ultramafic pseudotachylyte veins that we sampled, away from fractures, do not display any color variation from margin to center, a characteristic demonstrating the lack of alteration/serpentinization in our samples; and (iii) the magnetite grains observed in thin section in our samples are not spatially associated with any hydrous phases, which precludes a serpentinization origin (Figure 1).

In summary, although the exact magnetite concentration of the host peridotites before seismic slip (i.e., pseudotachylyte formation) remains uncertain, the low fO_2 calculated for unaltered, nonmetasomatic upper mantle rocks (Frost & McCammon, 2008; Woodland & Koch, 2003) would allow only small concentrations of magnetite to form in mantle peridotites.

5.2. Magnetite in Natural and Artificial Ultramafic Pseudotachylytes

In this study, we did not attempt to correlate magnetite grain size with vein thickness because many factors, including cooling rate and melt flow rate, will affect granulometry in sheet-like intrusions.

Previous petrologic studies of natural fault pseudotachylytes have shown that frictional melting occurs under disequilibrium conditions, through selective melting of phases that have lower individual melting temperatures (e.g., Boullier et al., 2001; Camacho et al., 1995; Ferré et al., 2012; Patro et al., 2011; Zechmeister et al., 2007). Similar conditions prevail in artificial pseudotachylytes produced in frictional experiments (e.g., Del Gaudio et al., 2009; Nakamura et al., 2002). The main reason for frictional melting to take place out of equilibrium is the extremely short time frame of this process (e.g., Andersen & Austrheim, 2006).

The clast-to-matrix ratio in pseudotachylytes is, in first approximation, a good proxy for degree of melting, particularly when this ratio remains macroscopically relatively constant along a vein (e.g., Lin, 2008). In the ultramafic veins from the three investigated localities, this ratio generally ranges between 5 and 10%, which implies a high degree of melting (90 to 95%). Modal abundances of clinopyroxene, orthopyroxene, and olivine account for about 15, 15, and 70%, respectively, in modal abundance in a typical lherzolite. The predicted order in which mineral phases would melt under disequilibrium conditions follows increasing individual melting temperatures (for pure end members); i.e., at 1 atm, clinopyroxene (diopside) = 1,391°C; orthopyroxene (enstatite) = 1,557°C; magnetite = 1,597°C; olivine-Fo_{92} = 1,850°C; and chrome spinel = 2,200°C (e.g., Deer et al., 1992). These melting temperatures depend not only on the chemical composition of minerals but also in the case of frictional melts, on their mechanical properties such as fracture toughness (Kc) and Mohs numbers (Spray, 2010). The same melting order would persist at pressures up to 1 GPa, at which melting temperatures increase by about 50°C (Boyd & England, 1963; Boyd et al., 1964; Davis & England, 1964; Williams & Kennedy, 1969). The two phases that would predictably remain below the liquidus at the 90–95% degree of melting are chrome spinel and olivine. The selective character of melting is confirmed by the observation that survivor clasts in the ultramafic pseudotachylytes we studied dominantly consist of chrome spinel and olivine. The low clast/matrix ratio, along with the survival of unmolten olivine-Fo_{92} and chrome spinel clasts, constrains the melting temperature (T_M) of our natural pseudotachylytes to $<$1,850°C. Olivine rim compositions from artificial ultramafic pseudotachylytes (1 atm) provide a strong constraint on T_M at ≈1,780°C (Del Gaudio et al., 2009). Natural ultramafic pseudotachylytes formed under confining pressures $>$1 atm would have $T_M > 1{,}780$°C. The estimated T_M range (1,780–1,850°C) is at least 150°C above the melting temperature of magnetite, and therefore, a logical deduction is that any inherited small-size magnetite clasts having formed by frictional comminution predominantly would have readily melted. If magnetite had been encapsulated into forsterite olivine at a temperature between 1,597 and 1,850°C, it may have survived frictional melting. However,

all the magnetite grains identified in the ultramafic pseudotachylytes of this study were found exclusively within the matrix and not in clasts, which strongly supports a melt origin for these magnetite grains. In summary, the total of observations made is consistent with the argument that all magnetite present in ultramafic pseudotachylytes did not originate from inherited clasts and instead formed either during or after seismic slip.

Generally, frictional melting leads to the fusion of iron-bearing minerals (e.g., Allen et al., 2002; Obata & Karato, 1995), a process that liberates iron into the melt phase. This process is particularly significant in ultramafic pseudotachylytes because they originate from iron-rich rocks (≈9% FeO; supporting information Table S1) and therefore potentially constitute the most iron-rich frictional melts. All the mineral phases present in the peridotitic host rock before seismic slip contain iron. The fate of liberated iron depends, to a large extent, on fO_2 in the slip zone. With low fO_2, iron could theoretically form wüstite or combine with sulfur to form sulfides. Although Ueda et al. (2008) reported minor Fe-Ni sulfides in the A-type Balmuccia ultramafic pseudotachylyte (Figure 1c), wüstite has never been documented in such rocks. At slightly higher fO_2, liberated iron could form ilmenite, depending on titanium available in the system. Ilmenite has been described in eclogitic and gabbroic pseudotachylytes (Deseta et al., 2014a; Steltenpohl et al., 2006) but not in ultramafic pseudotachylytes. At still higher fO_2, liberated iron could form magnetite, an oxide that has been identified petrographically in previous studies of ultramafic pseudotachylytes, and we have thoroughly documented its presence with rock magnetic experiments in this study. Finally, the highest fO_2 conditions would lead to the formation of magmatic hematite (e.g., Petrik et al., 2003).

The host rock major element compositions and theoretical maximum values for the paramagnetic susceptibility (K_{para} values) are strikingly similar among the three studied localities (supporting information Table S1). Because the host mantle peridotites have relatively small MnO concentrations (≈0.13 wt %), K_{para} values primarily represents the maximum potential contribution of iron to form magnetic mineral phases. Because the FeO_t wt % of the host rock is relatively uniform (FeO_t = 8.0–9.3 wt %, average = 8.9 ± 0.3 wt %, n = 22), differences in the magnetic properties of the studied pseudotachylytes cannot be attributed to variations in host rock composition. Instead, these differences must reflect distinct physical conditions during or after pseudotachylyte formation.

The magnetic properties of the studied ultramafic pseudotachylytes, similar to pseudotachylytes formed from protoliths of other compositions (e.g., Ferré et al., 2012; Ferré, Friedman, et al., 2014 and Ferré, Geissman, et al., 2014), display a remarkable homogeneity. This consistency reflects the fact that despite the microstructural complexity of pseudotachylyte veins, frictional melts are produced all along the slip plane and their compositions average that of a relatively large volume of host rock.

All the rock magnetic results (Curie temperature, field of magnetic saturation, and hysteresis properties; Figure 3 and supporting information Figure S1) from the three ultramafic pseudotachylyte localities show that low-Ti magnetite is chiefly responsible for the ferromagnetic behavior of these rocks. The low Ti content of magnetite ($x_{ulv} < 2.1\%$), as determined by EDS spot analyses and thermomagnetic experiments, supports an origin for this mineral from the fusion of mafic silicates, instead of an origin from serpentinization, because the latter process produces purely stoichiometric (Ti-free) magnetite (e.g., Beard et al., 2009).

The origin of magnetite in the studied natural and artificial ultramafic pseudotachylytes should also be considered in the context of direct observations. Optical (petrographic) microscopy and scanning electron microscopy observations on the ultramafic pseudotachylytes (Figure 1) consistently show that (1) magnetite grains are of fairly uniform physical grain size (3–5 μm) at the scale of a thin section; (2) the grain size of magnetite in the veins is small (SD to PSD), which supports an origin from melting rather than serpentinization because the later tends to produce coarser (MD) grain sizes (e.g., Maffione et al., 2014); (3) the distribution of magnetite grains is relatively uniform, like in the artificial pseudotachylytes of Nakamura et al. (2002); and (4) magnetite grains occur within the matrix and are not spatially associated with any secondary serpentine or other hydrous phases. All these observations rule out an origin from metamorphic reactions involving fluids, such as serpentinization. Further, friction experiments under uncontrolled atmospheres consistently show that regardless of protolith composition, small subhedral magnetite grains form through breakdown of mafic silicates, followed by liberation of iron in the melt and subsequent oxidation of this iron (e.g., Nakamura et al., 2002; Del Gaudio et al., 2009).

5.3. Significance of Magnetite Grain Size and Abundance Variations in Ultramafic Pseudotachylytes

Magnetite grain size in ultramafic pseudotachylyte samples is evaluated using the Dunlop (2002) plot, which was modified after Day et al. (1977). The hysteresis parameters of a specimen depend on the mean magnetite grain size and are somewhat biased toward coarser grains; therefore they do not represent grain size distribution very accurately. However, useful information regarding magnetic granulometry can be provided by the representative FORC diagrams (Figure 4). The Balmuccia A-type specimens show the greatest variation of magnetic hysteresis properties (Figure 3), and this variation is tentatively interpreted as mixing of single domain (SD) and superparamagnetic (SP) grains. The other groups display relatively consistent hysteresis properties within each locality, with a significant overlap between samples from Monte Moncuni and Cima di Gratera. The Balmuccia B-type specimens show distinctively larger grain sizes in the pseudo-single domain (PSD) field. All the groups, with the exception of Balmuccia A-type, define broad arrays that are indicative of mixing between SD and PSD grain sizes (e.g., Carter-Stiglitz et al., 2001). None of the populations display dominance by multidomain (MD) grain sizes, as would be expected from a serpentinization origin. The significant difference in grain sizes between localities could be attributed to magnetite formation occurring under distinct fO_2 (high fO_2 would promote larger grain sizes), and/or under distinct cooling/quenching conditions (slower cooling would promote larger grain sizes), both of these would have a controlling effect upon growth rates. The three specimens of artificial ultramafic pseudotachylytes produced in experiments also define a mixing trend along a SD-PSD mixing line and are characterized by relatively large grain sizes compared to other groups (Figure 3). Because these artificial specimens are undoubtedly those that cooled the fastest, we interpret their relatively larger grain sizes as due to crystallization under the highest fO_2. Figure 2 shows that the concentration of magnetite (in ppm) is uniform within each group, including the artificial pseudotachylytes. The difference in magnetite abundance between the two Balmuccia groups is particularly revealing, because the Balmuccia A group, which formed at the greatest depth (pressure ≈ 1.0–1.3 GPa and T_A ≈ 1,100 K; Obata & Karato, 1995), clearly shows lower magnetite content than the shallower depth group, Balmuccia B-type (pressure ≈ 0.15–0.30 GPa and T_A ≈ 450–600 K; Souquière & Fabbri, 2010). Pseudotachylytes formed at deeper conditions would cool at a slower rate than shallower ones and would be expected to form larger magnetite grains, while magnetite abundance should primarily be determined by Fe concentration in the melt. Hence, the difference in magnetite abundance between Balmuccia A and B groups cannot reflect the effect of different cooling rates. Instead, this stark contrast is better explained if Balmuccia A-type pseudotachylytes formed under low fO_2 at great depth (≈30–40 km), whereas Balmuccia B-type formed under higher fO_2 at shallow depth (≈5–10 km).

6. Conclusions

Our magnetic and microscopic observations show that natural and artificial ultramafic pseudotachylytes (that is, pseudotachylytes hosted by mantle ultramafic rocks) contain low-Ti magnetite, of a relatively uniform coercivity, as the dominant ferromagnetic (*s.l.*) phase. Magnetic methods are particularly well suited to investigate variations in magnetite content at low concentrations, because magnetite is distinct from Fe-Mg silicates due to its high magnetic remanence and magnetic susceptibility. The magnetite populations we document and describe formed primarily from the fusion of mafic silicates such as olivine and pyroxenes, a process that liberated iron in the frictional melt, and was followed by oxidation to produce Fe_3O_4. We show that the bulk of magnetite grains in ultramafic pseudotachylytes cannot have been inherited from unmolten clasts of the peridotitic host rocks, because the temperatures involved are ≈150°C higher than the melting point of magnetite. We also show that the magnetite grains present in the pseudotachylytes we studied did not form by serpentinization after seismic events, because our specimens are free of secondary serpentinization. Finally and most importantly, we hypothesize that the large differences in magnetite abundance and magnetite grain size are best explained by pseudotachylyte formation under variable oxygen fugacities, either at depths of ≈30–40 km (low fO_2) or at shallower depths of 5–10 km (high fO_2). Therefore, the magnetic properties of fault-related ultramafic pseudotachylytes provide a crude proxy for their depth of formation and will be useful to assess their tectonic significance. In the specific case of Balmuccia, where at least two successive sets of ultramafic pseudotachylytes coexist, the deeper pseudotachylytes we propose could have formed at depths typical of continental lithosphere crust-mantle (Moho) depths, during Carboniferous-Permian time, once the Balmuccia ultramafic lens was already part of the lower continental crust. In

contrast, the shallower pseudotachylytes we propose could have formed at upper crustal depths, during the late Eocene Alpine exhumation.

Acknowledgments
We kindly acknowledge the hospitality of many local residents in the villages of Alagna in Val Sesia, Trana in Alpi Cozie, and Patrimonio in Corsica. The Centre for Earth Evolution and Dynamics at UiO is funded by CoE-grant 223272 from the Research Council of Norway. The magnetic measurements performed at SIU were performed on instrumentation funded by NSF grant EAR-0521558 to ECF. The magnetic data are accessible from the MagIC database at https://www2.earthref.org/MagIC. The Editor Michael Walter, Associate Editor Mark Dekkers, and two anonymous reviewers are kindly acknowledged for their detailed review of this manuscript.

References

Allen, J. L., O'Hara, K. D., & Moecher, D. P. (2002). Structural geometry and thermal history of pseudotachylyte from the Homestake shear zone, Sawatch Range, Colorado. In D. Lageson (Ed.), *Field Guide 3* (Vol. 3, pp. 17–32). Washington: Geological Society of America.

Andersen, T. B., & Austrheim, H. (2006). Fossil earthquakes recorded by pseudotachylytes in mantle peridotite from the Alpine subduction complex of Corsica. *Earth and Planetary Science Letters*, *242*(1-2), 58–72. https://doi.org/10.1016/j.epsl.2005.11.058

Andersen, T. B., Mair, K., Austrheim, H., Podladchikov, Y. Y., & Vrijmoed, J. C. (2008). Stress release in exhumed intermediate and deep earthquakes determined from ultramafic pseudotachylyte. *Geology*, *36*(12), 995–998. https://doi.org/10.1130/G25230A.1

Andersen, T. B., Austrheim, H., Deseta, N., Silkoset, P., & Ashwal, L. D. (2014). Large subduction earthquakes along the fossil Moho in Alpine Corsica. *Geology*, *42*(5), 395–398. https://doi.org/10.1130/G35345.35341

Austrheim, H., & Andersen, T. B. (2004). Pseudotachylytes from Corsica: Fossil earthquakes from a subduction complex. *Terra Nova*, *16*(4), 193–197. https://doi.org/10.1111/j.1365-3121.2004.00551.x

Aydin, A., Ferré, E. C., & Aslan, Z. (2007). The magnetic susceptibility of granitic rocks as a proxy for geochemical differentiation: Example from the Saruhan granitoids, NE Turkey. *Tectonophysics*, *441*(1-4), 85–95. https://doi.org/10.1016/j.tecto.2007.04.009

Beard, J. S., Frost, B. R., Fryer, P., McCaig, A., Searle, R., Ildefonse, B., … Sharma, S. K. (2009). Onset and progression of serpentinization and magnetite formation in olivine-rich troctolite from IODP Hole U1309D. *Journal of Petrology*, *50*(3), 387–403. https://doi.org/10.1093/petrology/egp004

Boullier, A.-M., Ohtani, T., Fujimoto, K., Ito, H., & Dubois, M. (2001). Fluid inclusions in pseudotachylytes from the Nojima fault, Japan. *Journal of Geophysical Research*, *106*(B10), 21965–21977. https://doi.org/10.1029/2000JB000043

Boyd, F. R., & England, J. L. (1963). Effect of pressure on the melting of diopside, $CaMgSi_2O_6$, and albite, $NaAlSi_3O_8$, in the range up to 50 kilobars. *Journal of Geophysical Research*, *68*(1), 311–323. https://doi.org/10.1029/JZ068i001p00311

Boyd, F. R., England, J. L., & Davis, B. T. C. (1964). Effects of pressure on the melting and polymorphism of enstatite, $MgSiO_3$. *Journal of Geophysical Research*, *69*(10), 2101–2109. https://doi.org/10.1029/JZ069i010p02101

Camacho, A., Vernon, R. H., & Fitz Gerald, J. D. (1995). Large volumes of anhydrous pseudotachylyte in the Woodroffe Thrust, eastern Musgrave Ranges, Australia. *Journal of Structural Geology*, *17*(3), 371–383. https://doi.org/10.1016/0191-8141(94)00069-C

Carter-Stiglitz, B., Moskowitz, B., & Jackson, M. (2001). Unmixing magnetic assemblages and the magnetic behavior of bimodal mixtures. *Journal of Geophysical Research*, *106*(B11), 26397–26411. https://doi.org/10.1029/2001JB000417

Davis, B. T. C., & England, J. L. (1964). The melting of forsterite up to 50 kilobars. *Journal of Geophysical Research*, *69*(6), 1113–1116. https://doi.org/10.1029/JZ069i006p01113

Day, R., Fuller, M., & Schmidt, V. A. (1977). Hysteresis properties of titanomagnetites: Grain-size and compositional dependence. *Physics of the Earth and Planetary Interiors*, *13*(4), 260–267. https://doi.org/10.1016/0031-9201(77)90108-X

Deer, W. A., Howie, R. A., & Zussman, J. (1992). *The rock-forming minerals* (696 pp.). London: Longmans.

Del Gaudio, P., Di Toro, G., Han, R., Hirose, T., Nielsen, S., Shimamoto, T., & Cavallo, A. (2009). Frictional melting of peridotite and seismic slip. *Journal of Geophysical Research*, *114*, B06306. https://doi.org/10.1029/2008JB005990

Demouchy, S., Jacobsen, S. D., Gaillard, F., & Stern, C. R. (2006). Rapid magma ascent recorded by water diffusion profiles in mantle olivine. *Geology*, *34*(6), 429–432. https://doi.org/10.1130/G22386.1

Deseta, N., Andersen, T. B., & Ashwal, L. D. (2014a). A weakening mechanism for intermediate-depth seismicity? Detailed petrographic and microtextural observations from blueschist facies pseudotachylytes, Cape Corse, Corsica. *Tectonophysics*, *610*, 138–149. https://doi.org/10.1016/j.tecto.2013.11.007

Deseta, N., Ashwal, L. D., & Andersen, T. B. (2014b). Initiating intermediate-depth earthquakes: Insights from a HP–LT ophiolite from Corsica. *Lithos*, *206-207*, 127–146. https://doi.org/10.1016/j.lithos.2014.07.022

Di Toro, G., Nielsen, S., & Pennachioni, G. (2005). Earthquake rupture dynamics frozen in exhumed ancient faults. *Nature*, *436*(7053), 1009–1012. https://doi.org/10.1038/nature03910

Di Toro, G., Niemeijer, A. e., Tripoli, A., Nielsen, S., Di Felice, F., Scarlato, P., … Mariano, S. (2010). From field geology to earthquake simulation: A new state-of-the-art tool to investigate rock friction during the seismic cycle (SHIVA). *Rendiconti Lincei*, *21*(S1), 95–114. https://doi.org/10.1007/s12210-010-0097-x

Dunlop, D. J. (2002). Theory and application of the Day plot (M_{rs}/M_s versus H_{cr}/H_c). 1. Theoretical curves and tests using titanomagnetite data. *Journal of Geophysical Research*, *107*(B3), 2056. https://doi.org/10.1029/2001JB000486

Dunlop, D. J., & Özdemir, Ö. (2009). Magnetizations in rocks and minerals. In M. Kono (Ed.), *Geomagnetism* (Vol. 5, pp. 277–336). Amsterdam: Elsevier.

Evans, M. E., & Heller, F. (2003). *Environmental Magnetism: Principles and Applications of Enviromagnetics* (299 pp.). Amsterdam: Academic Press.

Facer, J., Downes, H., & Beard, A. (2009). In situ Serpentinization and hydrous fluid Metasomatism in spinel dunite xenoliths from the Bearpaw Mountains, Montana, USA. *Journal of Petrology*, *50*(8), 1443–1475. https://doi.org/10.1093/petrology/egp037

Feinberg, H., Horen, H., Michard, A., & Saddiqi, O. (1999). Obduction-related remagnetization at the base of an ophiolite: Paleomagnetism of the Samail nappe lower sequence and its continental substratum, southeast Oman Mountains. *Journal of Geophysical Research*, *104*(B8), 17,703–17,714. https://doi.org/10.1029/1999JB900171

Ferré, E. C., Tikoff, B., & Jackson, M. (2005a). The magnetic anisotropy of mantle peridotites: Example from the Twin Sisters dunite, Washington. *Tectonophysics*, *398*(3-4), 141–166. https://doi.org/10.1016/j.tecto.2005.02.001

Ferré, E. C., Tikoff, B., & Jackson, M. (2005b). Corrigendum to "The magnetic anisotropy of mantle peridotites: Example from the Twin Sisters dunite, Washington" [Tectonophysics 398 (2005) 141–166]. *Tectonophysics*, *405*(1-4), 233–233. https://doi.org/10.1016/j.tecto.2005.06.001

Ferré, E. C., Zechmeister, M. S., Geissman, J. W., MathanaSekaran, N., & Kocak, K. (2005). The origin of high magnetic remanence in fault pseudotachylites: Theoretical considerations and implication for coseismic electrical currents. *Tectonophysics*, *402*(1-4), 125–139. https://doi.org/10.1016/j.tecto.2005.01.008

Ferré, E. C., Geissman, J. W., & Zechmeister, M. S. (2012). Magnetic properties of fault pseudotachylytes in granites. *Journal of Geophysical Research*, *117*, B01106. https://doi.org/10.1029/2011JB008762

Ferré, E. C., Friedman, S. A., Martín-Hernández, F., Feinberg, J. M., Conder, J. A., & Ionov, D. A. (2013). The magnetism of mantle xenoliths and potential implications for sub-Moho magnetic sources. *Geophysical Research Letters*, *40*, 105–110. https://doi.org/10.1029/2012GL054100

Ferré, E. C., Friedman, S. A., Martin-Hernandez, F., Feinberg, J. M., Till, J. L., Ionov, D. A., & Conder, J. A. (2014). Eight good reasons why the uppermost mantle could be magnetic. *Tectonophysics*, *624-625*, 3–14. https://doi.org/10.1016/j.tecto.2014.01.004

Ferré, E. C., Geissman, J. W., Demory, F., Gattacceca, J., Zechmeister, M., & Hill, M. J. (2014). Coseismic magnetization of fault pseudotachylytes: 1. Thermal demagnetization experiments. *Journal of Geophysical Research: Solid Earth*, *119*, 6113–6135. https://doi.org/10.1002/2014JB011168

Ferré, E. C., Chou, Y.-M., Kuo, R. L., Yeh, E.-C., Leibovitz, N. R., Meado, A. L., … Geissman, J. W. (2016). Deciphering viscous flow of frictional melts with the mini-AMS method. *Journal of Structural Geology*, *90*, 15–26. https://doi.org/10.1016/j.jsg.2016.1007.1002

Friedman, S. A., Feinberg, J. M., Ferré, E. C., Demory, F., Martin-Hernandez, F., Conder, J. A., & Rochette, P. (2014). Craton vs. rift uppermost mantle contributions to magnetic anomalies in the United States interior. *Tectonophysics*, *624-625*, 15–23. https://doi.org/10.1016/j.tecto.2014.04.023

Frost, D. J., & McCammon, C. A. (2008). The redox state of Earth's mantle. *Annual Review of Earth and Planetary Sciences*, *36*(1), 389–420. https://doi.org/10.1146/annurev.earth.36.031207.124322

Frost, B. R., Evans, K. A., Swapp, S. M., Beard, J. S., & Mothersole, F. E. (2013). The process of serpentinization in dunite from New Caledonia. *Lithos*, *178*(0), 24–39. https://doi.org/10.1016/j.lithos.2013.02.002

Goncharov, A. G., Ionov, D. A., & Doucet, L. S. (2012). Thermal state, oxygen fugacity and C-O-H fluid speciation in cratonic lithospheric mantle: New data on peridotite xenoliths from the Udachnaya kimberlite, Siberia. *Earth and Planetary Science Letters*, *357*, 99–110. https://doi.org/10.1016/j.epsl.2012.09.016

Handy, M. R., & Stünitz, H. (2002). Strain localization by fracturing and reaction weakening—A mechanism for initiating exhumation of subcontinental mantle beneath rifted margins. In S. De Meer, et al. (Eds.), *Deformation mechanisms, rheology and tectonics: Current status and future perspectives*. *Geological Society of London Special Publication*, 200, 387–407.

Hyndman, R. D., & Peacock, S. M. (2003). Serpentinization of the forearc mantle. *Earth and Planetary Science Letters*, *212*(3-4), 417–432. https://doi.org/10.1016/S0012-821X(03)00263-2

Jin, D., Karato, S. I., & Obata, M. (1998). Mechanisms of shear localization in the continental lithosphere: Inference from the deformation microstructures of peridotites from the Ivrea zone, northwestern Italy. *Journal of Structural Geology*, *20*(2-3), 195–209. https://doi.org/10.1016/S0191-8141(97)00059-X

John, T., & Schenk, V. (2006). Interrelations between intermediate-depth earthquakes and fluid flow within subducting oceanic plates: Constraints from eclogite facies pseudotachylytes. *Geology*, *34*(7), 557–560. https://doi.org/10.1130/G22411.1

Kanamori, H., Anderson, D. L., & Heaton, T. H. (1998). Frictional melting during the rupture of the 1994 Bolivian earthquake. *Science*, *279*(5352), 839–842. https://doi.org/10.1126/science.279.5352.839

Kelley, K. A., & Cottrell, E. (2009). Water and the oxidation state of subduction zone magmas. *Science*, *325*(5940), 605–607. https://doi.org/10.1126/science.1174156

Kinman, W. S., & Neal, C. R. (2006). Magma evolution revealed by anorthite-rich plagioclase cumulate xenoliths from the Ontong Java Plateau: Insights into LIP magma dynamics and melt evolution. *Journal of Volcanology and Geothermal Research*, *154*(1-2), 131–157. https://doi.org/10.1016/j.jvolgeores.2005.09.024

Kohlstedt, D. L., Goetze, C., Durham, W. B., & Sande, J. V. (1976). New technique for decorating dislocations in olivine. *Science*, *191*(4231), 1045–1046. https://doi.org/10.1126/science.191.4231.1045

Lagroix, F., & Borradaile, G. J. (2000). Magnetic fabric interpretation complicated by inclusions in mafic silicates. *Tectonophysics*, *325*(3-4), 207–225. https://doi.org/10.1016/S0040-1951(00)00125-6

Lahondère, D. (1988). Eclogitic metamorphism in Farinoles orthogneisses and ophiolitic metabasites (northern Corsica, France). *Bulletin de la Société Géologique de France*, *4*, 579–585.

Lin, A. (2008). *Fossil earthquakes: The formation and preservation of pseudotachylytes* (345 pp.). Berlin: Springer, Lecture Notes in Earth Sciences.

Maddock, R. H. (1983). Melt origin of pseudotachylites demonstrated by textures. *Geology*, *11*(2), 105–108. https://doi.org/10.1130/0091-7613(1983)11%3C105:MOOFPD%3E2.0.CO;2

Maffione, M., Morris, A., Plümper, O., & van Hinsbergen, D. J. J. (2014). Magnetic properties of variably serpentinized peridotites and their implication for the evolution of oceanic core complexes. *Geochemistry, Geophysics, Geosystems*, *15*, 923–944. https://doi.org/10.1002/2013GC004993

Magott, R., Fabbri, O., & Fournier, M. (2016). Subduction zone intermediate-depth seismicity: Insights from the structural analysis of Alpine high-pressure ophiolite-hosted pseudotachylyte (Corsica, France). *Journal of Structural Geology*, *87*, 95–114. https://doi.org/10.1016/j.jsg.2016.04.002

Magott, R., Fabbri, O., & Fournier, M. (2017). Polyphase ductile/brittle deformation along a major tectonic boundary in an ophiolitic nappe, Alpine Corsica: Insights on subduction zone intermediate-depth asperities. *Journal of Structural Geology*, *94*, 240–257. https://doi.org/10.1016/j.jsg.2016.12.002

Malvoisin, B., Carlut, J., & Brunet, F. (2012). Serpentinization of oceanic peridotites: 1. A high-sensitivity method to monitor magnetite production in hydrothermal experiments. *Journal of Geophysical Research*, *117*, B01104. https://doi.org/10.1029/2011JB008612

Martin-Hernandez, F., Ferré, E. C., & Friedman, S. A. (2014). Remanent magnetization in fresh xenoliths derived from combined demagnetization experiments: Magnetic mineralogy, origin and implications for mantle sources of magnetic anomalies. *Tectonophysics*, *624-625*, 24–31. https://doi.org/10.1016/j.tecto.2014.04.006

Matysiak, A. K., & Trepmann, C. A. (2012). Crystal-plastic deformation and recrystallization of peridotite controlled by the seismic cycle. *Tectonophysics*, *530-531*, 111–127. https://doi.org/10.1016/j.tecto.2011.11.029

Maxbauer, D. P., Feinberg, J. M., & Fox, D. L. (2016). MAX UnMix: A web application for unmixing magnetic coercivity distributions. *Computers & Geosciences*, *95*, 140–145. https://doi.org/10.1016/j.cageo.2016.07.009

Moody, J. B. (1976). Serpentinization: A review. *Lithos*, *9*(2), 125–138. https://doi.org/10.1016/0024-4937(76)90030-X

Nakamura, N., Hirose, T., & Borradaile, G. J. (2002). Laboratory verification of submicron magnetite production in pseudotachylytes: Relevance for paleointensity studies. *Earth and Planetary Science Letters*, *201*(1), 13–18. https://doi.org/10.1016/S0012-821X(02)00704-5

Nielsen, S. (2011). Istituto Nazionale di Geofisica e Vulcanologia, Earthquake fault dynamics: Insights from laboratory experiments. Presented at the Proceedings Società Italiana di Fisica.

Niemeijer, A., Di Toro, G., Nielsen, S., & Di Felice, F. (2011). Frictional melting of gabbro under extreme experimental conditions of normal stress, acceleration, and sliding velocity. *Journal of Geophysical Research*, *116*, B07404. https://doi.org/10.1029/2010JB008181

Nixon, P. H. (1987). *Mantle xenoliths* (844 pp.). Chichester: John Wiley.

Obata, M., & Karato, S. (1995). Ultramafic pseudotachylite from the Balmuccia peridotite, Ivrea-Verbano zone, northern Italy. *Tectonophysics*, *242*(3-4), 313–328. https://doi.org/10.1016/0040-1951(94)00228-2

O'Driscoll, B., & Petronis, M. S. (2009). Oxide mineral formation during the serpentinization of a Cr-spinel seam: Insights from rock magnetic experiments. *Geochemistry, Geophysics, Geosystems*, *10*, Q01008. https://doi.org/10.1029/2008GC002274

Patro, R., Mahapatro, S. N., Bhattacharya, A., Pant, N. C., Nanda, J. K., Dey, A., & Tripathy, A. K. (2011). Chemical heterogeneity in an enderbite-hosted pseudotachylite, eastern India: Evidence for syn-deformation multi-reaction melting in pseudotachylite. *Contributions to Mineralogy and Petrology*, *161*(4), 547–563. https://doi.org/10.1007/s00410-010-0548-5

Peslier, A. H., Woodland, A. B., & Wolff, J. A. (2008). Fast kimberlite ascent rates estimated from hydrogen diffusion profiles in xenolithic mantle olivines from southern Africa. *Geochimica et Cosmochimica Acta*, *72*(11), 2711–2722. https://doi.org/10.1016/j.gca.2008.03.019

Petrik, I., Nabelek, P. I., Janak, M., & Plasienka, D. (2003). Conditions of formation and crystallization kinetics of highly oxidized pseudotachylytes from the High Tatras (Slovakia). *Journal of Petrology*, *44*(5), 901–927. https://doi.org/10.1093/petrology/44.5.901

Piccardo, G. B., Ranalli, G., Marasco, M., & Padovano, M. (2007). Ultramafic pseudotachylytes in the Mt. Moncuni peridotite (Lanzo Massif, western Alps): Tectonic evolution and upper mantle seismicity. *Periodico di Mineralogia*, *76*, SPECIAL ISSUE: In honour of Ezio Callegari on his retirement, 181–197.

Piccardo, G. B., Ranalli, G., & Guarnieri, L. (2010). Seismogenic shear zones in the lithospheric mantle: Ultramafic pseudotachylytes in the Lanzo peridotite (Western Alps, NW Italy). *Journal of Petrology*, *51*(1-2), 81–100. https://doi.org/10.1093/petrology/egp067

Pittarello, L., Pennacchioni, G., & Di Toro, G. (2012). Amphibolite-facies pseudotachylytes in Premosello metagabbro and felsic mylonites (Ivrea Zone, Italy). *Tectonophysics*, *580*, 43–57. https://doi.org/10.1016/j.tecto.2012.08.001

Putnis, A. (1979). Electron petrography of high-temperature oxidation in olivine from the rhum layered intrusion. *Mineralogical Magazine*, *43*(326), 293–296. https://doi.org/10.1180/minmag.1979.043.326.12

Quick, J. E., Sinigoi, S., & Mayer, A. (1995). Emplacement of mantle peridotite in the lower continental crust, Ivrea-Verbano Zone, Northwest Italy. *Geology*, *23*(8), 739–742. https://doi.org/10.1130/0091-7613(1995)023%3C0739:EOMPIT%3E2.3.CO;2

Quick, J. E., Sinigoi, S., Snoke, A. W., Kalakay, T. J., Mayer, A., & Peressini, G. (2003). Geologic map of the Southern Ivrea–Verbano Zone, Northwestern Italy US Geological Survey I-Map 2003 v. 2776.

Ravna, E. J. K., Andersen, T. B., Jolivet, L., & De Capitani, C. (2010). Cold subduction and the formation of lawsonite eclogite—Constraints from prograde evolution of eclogitized pillow lava from Corsica. *Journal of Metamorphic Geology*, *28*(4), 381–395. https://doi.org/10.1111/j.1525-1314.2010.00870.x

Roberts, A. P., Heslop, D., Zhao, X., & Pike, C. R. (2014). Understanding fine magnetic particle systems through use of first-order reversal curve diagrams. *Reviews of Geophysics*, *52*, 557–602. https://doi.org/10.1002/2014RG000462

Rutter, E., Brodie, K., James, T., & Burlini, L. (2007). Large-scale folding in the upper part of the Ivrea-Verbano zone, NW Italy. *Journal of Structural Geology*, *29*(1), 1–17. https://doi.org/10.1016/j.jsg.2006.08.013

Shervais, J. W. (1979). Petrology and structure of the Alpine lherzolite massif at Balmuccia. Italy (PhD dissertation) (428 pp.). Santa Barbara: University of California.

Shervais, J. W., & Mukasa, S. B. (1991). The Balmuccia Orogenic Lherzolite Massif, Italy. *Journal of Petrology*, *Special_Volume*(2), 155–174. https://doi.org/10.1093/petrology/Special_Volume.2.155

Shimamoto, T., & Nagahama, H. (1992). An argument against the crush origin of pseudotachylytes based on the analysis of clast-size distribution. *Journal of Structural Geology*, *14*(8-9), 999–1006. https://doi.org/10.1016/0191-8141(92)90031-Q

Sibson, R. H. (1975). Generation of pseudotachylite by ancient seismic faulting. *Geophysical Journal of the Royal Astronomical Society*, *43*(3), 775–794. https://doi.org/10.1111/j.1365-246X.1975.tb06195.x

Sibson, R. H., & Toy, V. G. (2006). The habitat of fault-generated pseudotachylyte: Presence vs. absence of friction-melt. In R. Abercrombie, et al. (Eds.), *Earthquakes: Radiated energy and the physics of faulting* (Vol. 170, pp. 153–166). Washington, DC: American Geophysical Union. https://doi.org/10.1029/170GM16

Silkoset, P. (2013). Microtextures of ultramafic pseudotachylyte fault veins from Corsica an SEM-EBSD analysis (Master thesis) (196 pp.) University of Oslo.

Smith, D. (2010). Antigorite peridotite, metaserpentinite, and other inclusions within diatremes on the Colorado Plateau, SW USA: Implications for the mantle wedge during low-angle subduction. *Journal of Petrology*, *51*(6), 1355–1379. https://doi.org/10.1093/petrology/egq022

Souquière, F., & Fabbri, O. (2010). Pseudotachylytes in the Balmuccia peridotite (Ivrea Zone) as markers of the exhumation of the southern Alpine continental crust. *Terra Nova*, *22*(1), 70–77. https://doi.org/10.1111/j.1365-3121.2009.00918.x

Souquière, F., Monié, P., Fabbri, O., & Chauvet, A. (2011). Polyphase seismic faulting in the Ivrea zone (Italian Alps) revealed by 40Ar/39Ar dating of pseudotachylytes. *Terra Nova*, *23*(3), 162–170. https://doi.org/10.1111/j.1365-3121.2011.00994.x

Spray, J. G. (2010). Frictional melting processes in planetary materials: From hypervelocity impact to earthquakes. *Annual Review of Earth and Planetary Sciences*, *38*(1), 221–254. https://doi.org/10.1146/annurev.earth.031208.100045

Steltenpohl, M. G., Kassos, G., & Andresen, A. (2006). Retrograded eclogite-facies pseudotachylytes as deep-crustal paleoseismic faults within continental basement of Lofoten, north Norway. *Geosphere*, *2*(1), 61–72. https://doi.org/10.1130/GES00035.1

Syono, Y. (1960). Magnetic susceptibility of some rock forming silicate minerals such as amphiboles, biotites, cordierites and garnets. *Journal of Geomagnetism and Geoelectricity*, *11*(3), 85–93. https://doi.org/10.5636/jgg.11.85

Tanikawa, W., Mishima, T., Hirono, T., Soh, W., & Song, S.-R. (2008). High magnetic susceptibility produced by thermal decomposition of core samples from the Chelungpu fault in Taiwan. *Earth and Planetary Science Letters*, *272*(1-2), 372–381. https://doi.org/10.1016/j.epsl.2008.05.002

Tauxe, L. (1998). *Paleomagnetic principles and practice* (299 pp.). Dordrecht: Kluwer Academic, Modern approches in Geophysics.

Tauxe, L., Bertram, H. N., & Seberino, C. (2002). Physical interpretation of hysteresis loops: Micromagnetic modeling of fine particle magnetite. *Geochemistry, Geophysics, Geosystems*, *3*(10), 1–221055. https://doi.org/10.1029/2001GC000241

Taylor, L. A., & Neal, C. R. (1989). Eclogites with crustal and mantle signatures from the Bellsbank kimberlite, South Africa. Part 1: Mineralogy, petrography, and whole-rock geochemistry. *Journal of Geology*, *97*(5), 551–567. https://doi.org/10.1086/629334

Techmer, K. S., Ahrendt, H., & Weber, K. (1992). The development of pseudotachylyte in the Ivrea-Verbano Zone of the Italian Alps. *Tectonophysics*, *204*(3-4), 307–322. https://doi.org/10.1016/0040-1951(92)90314-V

Toft, P. B., Arkani-Hamed, J., & Haggerty, S. E. (1990). The effects of serpentinization on density and magnetic susceptibility: A petrophysical model. *Physics of the Earth and Planetary Interiors*, *65*(1-2), 137–157. https://doi.org/10.1016/0031-9201(90)90082-9

Ueda, T., Obata, M., Di Toro, G., Kanagawa, K., & Ozawa, K. (2008). Mantle earthquakes frozen in mylonitized ultramafic pseudotachylytes of spinel-lherzolite facies. *Geology*, *36*(8), 607–610. https://doi.org/10.1130/G24739A.1

Vitale-Brovarone, A., Beyssac, O., Malavielle, J., Molli, G., Beltrando, M., & Compagnoni, R. (2013). Stacking and metamorphism of continuous segments of subducted lithosphere in a high-pressure wedge: the example of Alpine Corsica (France). *Earth-Science Reviews*, *116*, 35e56. https://doi.org/10.1016/j.earscirev.2012.10.003

Wasilewski, P. J. (1987). Magnetic properties of mantle xenoliths and the magnetic character of the crust-mantle boundary. In P. H. Nixon (Ed.), *Mantle Xenoliths* (pp. 577–588). London: John Wiley.

Wasilewski, P. J., & Mayhew, M. A. (1992). The Moho as a magnetic boundary revisited. *Geophysical Research Letters*, *19*(22), 2259–2262. https://doi.org/10.1029/92GL01997

Wasilewski, P. J., Thomas, H. H., & Mayhew, M. A. (1979). The Moho as a magnetic boundary. *Geophysical Research Letters*, *6*(7), 541–544. https://doi.org/10.1029/GL006i007p00541

Williams, D. W., & Kennedy, G. C. (1969). Melting curve of diopside to 50 kilobars. *Journal of Geophysical Research*, *74*(17), 4359–4366. https://doi.org/10.1029/JB074i017p04359

Woodland, A. B., & Koch, M. (2003). Variation in oxygen fugacity with depth in the upper mantle beneath the Kaapvaal craton, Southern Africa. *Earth and Planetary Science Letters*, *214*(1-2), 295–310. https://doi.org/10.1016/S0012-821X(03)00379-0

Zechmeister, M. S., Ferré, E. C., Cosca, M. A., & Geissman, J. W. (2007). Slow and fast deformation in the Dora Maira Massif, Italian Alps: Pseudotachylytes and inferences on exhumation history. *Journal of Structural Geology*, *29*(7), 1114–1130. https://doi.org/10.1016/j.jsg.2007.03.009